PHYSICAL REVIEW D **88,** 023520 (2013)

Galactic structure explained with dissipative mirror dark matter

R. Foot*

ARC Centre of Excellence for Particle Physics at the Terascale, School of Physics, University of Melbourne, Victoria 3010, Australia

(Received 18 April 2013; published 18 July 2013)

Dissipative dark matter, such as mirror dark matter and related hidden-sector dark matter candidates, require an energy source to stabilize dark matter halos in spiral galaxies. It has been proposed previously that supernovae could be the source of this energy. Recently, it has been argued that this mechanism might explain two galactic scaling relations inferred from observations of spiral galaxies. One of these is that $\rho_0 r_0$ is roughly constant, and the other relates the galactic luminosity to r_0. (ρ_0 is the dark matter central density and r_0 is the core radius.) Here we derive equations for the heating of the halo via supernova energy, and the cooling of the halo via thermal bremsstrahlung. These equations are numerically solved to obtain constraints on the ρ_0, r_0 parameters appropriate for spiral galaxies. These constraints are in remarkable agreement with the aforementioned scaling relations.

DOI: 10.1103/PhysRevD.88.023520 PACS numbers: 95.35.+d

I. INTRODUCTION

The standard ΛCDM scenario [1], which invokes weakly interacting dark matter particles, has proven to be extremely successful in explaining the observed large-scale structure and cosmic microwave background anisotropies [2]. However, this scenario is challenged by observations on smaller scales. For example, measurements of rotation curves of spiral galaxies indicate the existence of a dark matter cored profile (e.g. Ref. [3]) in disagreement with the cuspy profile predicted by simulations of noninteracting dark matter [4].

Another challenge to the standard ΛCDM scenario is the lack of any evidence for new stable particles in LHC collider searches [5]. From a particle physics perspective, though, there is no compelling reason to favor weakly interacting particles over richer dark matter scenarios. In fact, the success of the standard model in explaining all collider data to date is a definite hint that dark matter resides in a hidden sector. That is, the fundamental Lagrangian decomposes into two sectors: one describing the standard particles and forces, and another which will contain the dark matter,

$$\mathcal{L} = \mathcal{L}_{\rm SM} + \mathcal{L}_{\rm dark}. \tag{1}$$

The sector describing the ordinary particles has $G = \mathrm{SU}(3) \otimes \mathrm{SU}(2)_L \otimes \mathrm{U}(1)_Y$ gauge symmetry, while the dark sector has independent gauge symmetries, G'. In this case one expects dark matter to be multicomponent, self-interacting and perhaps dissipative if the hidden sector has an unbroken $\mathrm{U}(1)'$ gauge symmetry. Such scenarios can also successfully explain the large-scale structure and cosmic microwave background (CMB), but can yield very different physics on small scales. Such hidden-sector dark matter has been discussed in the literature in a variety of contexts; see e.g. Refs. [6–20].

If the hidden sector does indeed contain an unbroken $\mathrm{U}(1)'$ gauge symmetry, then the associated "dark" photon can kinetically mix with the ordinary photon,

$$\mathcal{L}_{\rm mix} = \frac{\epsilon}{2} F^{\mu\nu} F'_{\mu\nu}, \tag{2}$$

where $F_{\mu\nu}$ ($F'_{\mu\nu}$) is the field-strength tensor for the photon (dark photon). Such kinetic mixing is gauge invariant and renormalizable [21] with ϵ viewed as a fundamental parameter of the theory. The physical effect of the kinetic mixing interaction [22] is to induce a tiny ordinary electric charge ($\propto \epsilon$) for the hidden sector $\mathrm{U}(1)'$ charged particles.

Mirror dark matter is a well-motivated and concrete example of hidden-sector dark matter in which $\mathcal{L}_{\rm dark}$ is an exact duplicate of the standard model sector [23]. This means that the hidden sector has gauge symmetry $G' = \mathrm{SU}(3)' \otimes \mathrm{SU}(2)'_L \otimes \mathrm{U}(1)'_Y$. If the chiral left- and right-handed fermion fields are interchanged in such a hidden sector then the theory has an unbroken "mirror" symmetry mapping each ordinary particle onto a "mirror" particle (along with $x \to -x$). That is, for each ordinary particle $e, \nu, u, d, \ldots, \gamma, \ldots$ there is a corresponding mirror particle, which we denote with a prime ($'$): $e', \nu', u', d', \ldots, \gamma', \ldots$. The unbroken mirror symmetry ensures that the mirror particles have the same masses as their corresponding ordinary counterparts. Similarly the gauge self-interactions (mirror electromagnetism, etc.) have the same form and strength in the mirror sector as they do in the ordinary sector. Although the focus here is on mirror dark matter, our results may be relevant to closely related hidden-sector models, such as the ones discussed in Ref. [15].

Mirror dark matter has emerged as an interesting dark matter candidate; for reviews and more complete bibliography see e.g. Ref. [8]. Mirror dark matter can explain [9] the large-scale structure of the Universe—the matter power

*rfoot@unimelb.edu.au

spectrum and CMB—in a manner analogous to standard collisionless cold dark matter models provided that $\epsilon \lesssim 10^{-9}$ [24]. Such values of ϵ are well consistent with direct laboratory limits, which arise from rare decays of orthopositronium [25]. Importantly, mirror dark matter can also explain [26] the positive dark matter signals from the DAMA [27] experiment along with the more tentative signals from the CoGeNT [28], CRESST-II [29] and CDMS/Si [30] direct detection experiments. This explanation requires photon-mirror photon kinetic mixing with a strength of $\epsilon \sim 10^{-9}$. Of course, this type of rich dark matter candidate can feature a whole range of phenomena, especially on small scales (galactic and smaller) which have only begun to be explored (see e.g. Refs. [31–36]).

In this article we return to the problem of galaxy structure in the context of mirror dark matter. The existence of the unbroken $U(1)'$ interaction will inevitably lead to significant self-interactions of the mirror particles. An implication of this is that galactic halos of spiral galaxies would have to be composed (predominately) of mirror particles in a pressure-supported spherical plasma [33]. There may also be a subcomponent consisting of compact objects such as old mirror stars. Some of the interactions within the halo will be dissipative, such as thermal bremsstrahlung (e.g. $e' + \mathrm{He}' \to e' + \mathrm{He}' + \gamma'$) which can cool the halo. At first sight, this might put into question the very existence of the halo. At any rate, the stability of the halo needs to be explained. A possible explanation was suggested sometime ago [33]. The idea is that ordinary core-collapse supernovae provide the required energy. In the hot and dense core of a type II supernova mirror electrons and positrons can be created from kinetic mixing-induced plasmon decay processes [37]. Thus ordinary supernovae can be a source of light mirror particles as well as the ordinary neutrinos. Indeed, it is estimated that mirror particles $(e', \bar{e}', \gamma')$ carry off roughly half of the core collapse supernova energy if $\epsilon \sim 10^{-9}$ [34,37]. A significant fraction of this energy can be absorbed by the mirror particle halo and thereby potentially replace the energy lost due to dissipative interactions. Order-of-magnitude estimates [33] suggested that the amount of heat generated roughly matched the energy dissipated for the Milky Way. The same mechanism could be responsible for stabilizing the halos in all spiral galaxies. If so, then matching the total heat supplied from ordinary supernovae to the energy dissipated suggests [38] a rough galactic scaling relation for spirals: $R_{\mathrm{SN}} \propto \rho_0^2 r_0^3$. Here, ρ_0, r_0 are the dark matter central mass density and core radius and R_{SN} is the galactic supernova rate. It was further suggested that the way in which energy from supernovae is distributed would lead to a cored dark matter distribution. It was argued that a second scaling relation, $\rho_0 r_0 \approx$ const, might be explained in this way [38].

The purpose of this article is to provide a more detailed numerical analysis of this whole picture. Let us mention at the outset that the problem of small-scale structure is a complicated one and the analysis performed here, although an improvement on the rough physical arguments of Refs. [33,38], still has some deficiencies. A number of assumptions are made, which would require further checks and refinements. More importantly, we do not attempt to evolve the galaxy from an early time to its present state, but rather see if we can at least explain some of the current properties of spiral galaxies.

This paper is structured as follows. In Sec. II we give a brief overview of the central idea: dissipative dark matter candidates like mirror dark matter (and by extension, closely related hidden-sector models) can have their halo's stabilized via supernova energy. In Sec. III we discuss the hydrostatic equilibrium condition, which we numerically solve to obtain the galactic temperature profile for several example spiral galaxies. In Sec. IV we consider the ionization state of the halo. The equations governing the ionization fractions of the mirror helium, mirror hydrogen and mirror metal components are given and numerically solved. In Sec. V we derive equations for the heating of the halo via supernova energy, and the cooling of the halo via thermal bremsstrahlung. These equations are numerically solved to obtain constraints on the ρ_0, r_0 parameters appropriate for spiral galaxies. These constraints are then compared with the scaling relations inferred from observations of galactic rotation curves. In Sec. VI, we comment on dwarf spheroidal galaxies and in Sec. VII we briefly discuss elliptical galaxies and galaxy clusters. Finally we give a few concluding remarks in Sec. VIII.

II. THE HEATING OF THE GALACTIC HALO

The physical picture is that spiral galaxies such as the Milky Way are currently composed of ordinary matter in a disk, and mirror dark matter predominantly in a (roughly) spherical halo. The halo consists of an ionized plasma formed out of the mirror particles, e', H', He', O', Fe', ... The plasma dissipates energy due to thermal bremsstrahlung and other processes and this energy needs to be replaced. The idea [33] is that ordinary supernovae can supply this required energy if photon-mirror photon kinetic mixing exists [Eq. (2)]. Such kinetic mixing gives the mirror electron and positron a tiny ordinary electric charge of magnitude ϵe. The energy-loss rate for production of such mini-charged particles from supernovae has been estimated in Ref. [37],

$$Q_P = \frac{8\zeta_3}{9\pi^3}\epsilon^2\alpha^2\left(\mu_e^2 + \frac{\pi^2 T^2}{3}\right)T^3 Q_1, \tag{3}$$

where Q_1 is a factor of order unity, and μ_e is the electron chemical potential and $T \approx 30$ MeV is the temperature of the supernova core. Demanding that Q_P does not exceed the energy loss rate due to neutrino emission implies that $\epsilon \lesssim 10^{-9}$ [37]. Thus, supernova can be a source of energetic light mirror particles e', $\bar{e}'$, γ' which can ultimately replace the energy lost due to radiative cooling. This

heating of the halo is in the central region of the galaxy, which leads to the temperature having a mild radial dependence. The halo is generally hotter at the center and decreases as the distance from the center, r, increases. The "average" halo temperature (say at a distance $r = 3r_D$ where r_D is the disk scale length) is typically of order 300 eV for the Milky Way, and ranges from 10 eV for the smallest spirals to around a few keV for the largest spirals (see the discussion in the following section).

The amount of supernova energy required to replace the halo energy lost due to radiative cooling is sizable. Estimates [33,38] indicate that at least a few percent of the total supernova energy needs to be absorbed by the halo. Is this reasonable? Let us assume a kinetic mixing parameter $\epsilon \sim 10^{-9}$, so that around half of type II supernova energy is converted into e', $\bar{e}'$, γ' emitted from the core initially with energies $\sim$ MeV. The huge number of energetic e', $\bar{e}'$, γ' particles injected into the region (~ 1 pc^3) around an ordinary supernova will rapidly cool, ultimately converting most of their energy into mirror photons. The energy spectrum of these mirror photons is naturally very difficult to predict but it could have some vague resemblance to the γ spectrum of ordinary gamma-ray bursts (GRBs). We recall that GRBs feature a fairly wide spectrum of energies with a mean of $\sim$700 keV with a few percent of the energy radiated below around 10 keV. In any case, these mirror photons will then heat the mirror-particle halo, potentially supplying the energy lost from the halo due to radiative cooling.

It has been argued previously [33,38] that this γ' energy cannot be transferred to the halo via elastic (Thomson) scattering off of free e''s in the plasma. The Thomson cross section is at least an order of magnitude too small. Thus, if the halo contains only H$'$ and He$'$ components, then it is hard to see how enough energy can be absorbed by the halo to replace the energy lost due to radiative cooling. However if the halo contains mirror metal components then the situation is much more promising. The heavy metal components are not fully ionized but can have their atomic K shells filled. The photoionization cross section is many orders of magnitude larger than the Thomson cross section and even a small metal component can make the halo optically thick, at least for a range of γ' energies. Once the energetic K shell e' is ejected from the ion, it will interact with the free e''s and the ions in the vicinity (typically $\sim$pc) and thermalize.

The total photoelectric cross section[1] of a mirror element with atomic number Z is given by (see e.g. Ref. [39])

$$\sigma_{\rm PE}(E_{\gamma'}) = \frac{g16\sqrt{2}\pi}{3m_e^2}\alpha^6 Z^5\left[\frac{m_e}{E_{\gamma'}}\right]^{7/2} \quad \text{for } E_{\gamma'} \gg I, \tag{4}$$

[1]Unless otherwise specified, we use natural units with $\hbar = c = 1$.

where I is the e' binding energy and $g = 1$ or 2 counts the number of K-shell mirror electrons present. Evidently, the photoelectric cross section decreases with mirror photon energy like $(E_{\gamma'})^{-7/2}$. For $E_{\gamma'}$ near threshold the cross section has a slightly softer behavior, $\sigma_{\rm PE} \propto 1/E_{\gamma'}^3$ and drops abruptly to zero at $E_{\gamma'} = I$ [40]. The contribution to the optical depth from such inelastic scattering for γ' propagating out from the galactic center is

$$\tau_{\rm IS} = \sum_{A'} 2\int_0^\infty \sigma_{\rm PE} n_{A'} dr \sim \sum_{A'} 2\rho_0 r_0 \sigma_{\rm PE}\left[\frac{\xi_{A'}}{m_{A'}}\right], \tag{5}$$

where $\xi_{A'}$ is the proportion by mass of the mirror metal component, A' (e.g. $A' = $ C$'$, O$'$, Si$'$, Fe$'$, ...). The quantities ρ_0 and r_0 are the halo central mass density and core radius, whose product $\rho_0 r_0$ has been inferred to be roughly constant (i.e. independent of galaxy luminosity), with a value around $10^{2.2} m_\odot/\text{pc}^2$ for a Burkert profile [41–43].

If we consider just the Fe$'$ component, we find that the optical depth is substantial, $\tau_{\rm IS} \gtrsim 0.1$, provided

$$E_{\gamma'} \lesssim 30 \text{ keV}\left[\frac{\rho_0 r_0}{10^{2.2} m_\odot/\text{pc}^2}\right]^{2/7}\left[\frac{\xi_{\text{Fe}'}}{0.05}\right]^{2/7}. \tag{6}$$

If the $\xi_{\text{Fe}'}$ component is not too small ($\gtrsim 0.01$) and assuming that the supernova γ' spectrum peaks above $\sim$30 keV and falls sharply at low energy (like a thermal spectrum) then the supernova energy being absorbed by the halo will arise (predominantly) from γ' in the energy range

$$9 \text{ keV} \lesssim E_{\gamma'} \lesssim 30 \text{ keV}. \tag{7}$$

Even if there are more abundant lighter components, such as O$'$, this may not change this picture greatly. Thus, including just the Fe$'$ component might be sufficient when considering how much supernova energy is being absorbed by the halo. We will see in Sec. V that the derived galactic scaling properties of spiral galaxies are relatively insensitive to the precise details of the supernova γ' spectrum.

To summarize, ordinary core-collapse supernova will produce light mirror particles e', $\bar{e}'$, γ' from their core with a total energy comparable to the neutrino burst provided that a kinetic mixing with a strength of $\epsilon \sim 10^{-9}$ exists. The bulk of this energy is expected to be converted into mirror photons, γ', in the region around the supernova. The details of the resulting γ' energy spectrum are poorly understood, but only the part of this spectrum below around 30 keV will be important for heating the halo. This heating is achieved by interactions (photoionization) with heavy mirror metal components, which occurs because these components retain their K-shell mirror electrons. Considering just Fe$'$ might be sufficient, as far as the heating of the halo is concerned, provided that the proportion of the supernova γ' energy spectrum below the Fe$'$ K-shell binding energy, ≈ 9 keV, is small.

III. HYDROSTATIC EQUILIBRIUM

The halo has two components: a plasma component and a dark disk/compact object component. Microlensing observations [44] provide some evidence that the mass of the plasma component dominates over that of the compact object component, and we henceforth focus on the plasma component.

The plasma component consists of a set of mirror particles, e', H$'$, He$'$, ... What is the *current* chemical composition of the halo? Early Universe cosmology suggests [45] that the primordial mirror helium mass fraction is around $Y^P \approx 0.9$ for $\epsilon \sim 10^{-9}$, with negligible primordial production of mirror metal components. In the first billion years or so, substantial mirror star formation and evolution is possible (currently, though, the halo is far too hot for much mirror star formation to occur). During this early period mirror metals could have been produced reasonably efficiently given that mirror stars with a large mirror helium mass fraction evolve 10–100 times faster than ordinary stars (which have $Y^P \approx 0.25$) [46]. Presumably this early epoch of mirror star formation is responsible for the current halo metal component (likely at least $\xi_{\mathrm{Fe}'} \gtrsim 0.01$) required for the halo to absorb enough of the mirror photons produced in the hot region around ordinary supernovae.[2] A significant halo metal component is also inferred from the mirror dark matter explanation [26] of the DAMA [27], CoGeNT [28] and CRESST-II [29] direct detection experiments. The end result is a halo currently composed primarily of He$'$ and H$'$, with He$'$ mass fraction around 0.9. Additionally there is a small metal fraction (a few percent by mass), which we take to be Fe$'$. An important quantity is the mean mass of the plasma particles,

$$\bar{m} \equiv \sum m_{A'} n_{A'} \Big/ \sum n_{A'}, \tag{8}$$

where $A' = e'$, H$'$, He$'$, Fe$'$ and $n_{A'}$ is the A' particle number density. For a fully ionized plasma, we estimate that $\bar{m} = 1.1$ GeV.

The set of mirror particles, e', H$'$, He$'$, ... in the plasma interact with each other via Coulomb scattering. These self-interactions suggest that mirror dark matter forms a pressure-supported halo. At the present time such a halo would be expected to be in hydrostatic equilibrium, where the force of gravity is balanced by the pressure gradient. That is,

$$\frac{dP}{dr} = -\rho(r) g(r) = -\bar{m} n_T(r) \frac{v_{\mathrm{rot}}^2}{r}, \tag{9}$$

where $\rho(r) = \bar{m} n_T(r)$, with $\bar{m}$ being the mean mass of the matter mirror particles defined in Eq. (8), $n_T(r)$ is the total dark matter particle number density[3] and $g(r)$ is the local acceleration due to gravity. Here $P(r) = n_T(r) T(r)$ and $v_{\mathrm{rot}}(r)$ is the local rotational velocity.

We shall assume that both the mirror particles and the ordinary baryons are distributed with spherical symmetry. Obviously in the central regions of spiral galaxies this might not be a good approximation, since the ordinary matter is distributed predominately in a disk. However so long as we consider $r \gtrsim r_D$, then the assumption of spherical symmetry could be reasonable. Furthermore, since the typical core radius of spirals is inferred to be somewhat larger than the disk scale length, r_D, it seems reasonable that the physics responsible for the existence and properties of the dark matter core will not depend too sensitively on the details of the mass distribution at $r \ll r_0$.

Anyway, with the assumption of spherical symmetry, g (and hence v_{rot}^2/r) can be related to the total mass density, ρ_{total}, via,

$$g(r) = \frac{G_{\mathrm{N}}}{r^2} \int_0^r \rho_{\mathrm{total}} dV, \tag{10}$$

where G_{N} is Newton's constant. The total mass density, ρ_{total}, can be separated into a contribution from ordinary baryons and one due to mirror particles. The baryonic contribution of spiral galaxies is approximated by a Freeman disk with surface density[4]

$$\Sigma = \frac{m_D}{2\pi r_D^2} e^{-r/r_D}, \tag{11}$$

where m_D is the disk mass and r_D is the disk scale length. Defining a spherically symmetric distribution, ρ_D, by requiring that the mass within a radius r is the same as that of the disk, i.e. $\int_0^r \rho_D 4\pi r'^2 dr' \equiv \int_0^r \Sigma 2\pi r' dr'$, we have

$$\rho_D(r) = \frac{m_D}{4\pi r_D^2 r} e^{-r/r_D}. \tag{12}$$

Studies of spiral galaxies have found that the baryonic mass m_D correlates with the disk radius r_D via [47,48]

[2]The rampant mirror star formation and evolution in the first few billion years or so of galactic evolution presumably included a large number of mirror supernovae. If the kinetic mixing interaction exists, then mirror supernovae should be a source of a large ordinary x-ray photon flux for the same reasons that ordinary supernovae are suspected to be a source of a large mirror x-ray photon flux. One could even speculate that these photons may have been responsible for the reionization of ordinary matter inferred from the CMB observations [2]. Importantly, the huge photon flux may not prevent the collapse of ordinary matter onto a disk because the ordinary matter with a negligible metal component (at that time) would absorb a relatively small fraction of the mirror supernovae energy.

[3]If we were to consider also a dark disk/compact object component made of old mirror stars, mirror white dwarfs, etc., then $n_T(r)$ in Eq. (9) would be just the plasma component of the halo.

[4]We do not include any other baryonic contribution other than the disk, so that m_D represents the total baryonic mass of the galaxy.

$$\log\left(\frac{r_D}{\mathrm{kpc}}\right) = 0.633 + 0.379\log\left(\frac{m_D}{10^{11}m_\odot}\right) + 0.069\left[\log\left(\frac{m_D}{10^{11}m_\odot}\right)\right]^2. \quad (13)$$

The philosophy adopted here is that the dark matter distribution within spiral galaxies is governed by hydrostatic equilibrium, dissipation and supernova heating. At the current epoch, these conditions might be sufficient to determine the dark matter density profile, independently of the past history of the galaxy. In the present work, though, we shall assume we know something about the form of the dark matter distribution (and justify this form later by showing that it is an approximate solution to the derived equations). We assume that dark matter can be approximated by a smooth cored distribution,

$$\rho_{\mathrm{dm}} = \bar{m}n_T(r) = \frac{\rho_0 r_0^3}{(r^2 + r_0^2)(r + r_0)}, \quad (14)$$

where r_0, ρ_0 are the dark matter core radius and central density respectively. Such a distribution, known as the Burkert profile, has been suggested by fits to rotation curves of spiral galaxies and other data [49]. Several scaling relations have been derived for ρ_0, r_0 from such data fitting. By adopting the same dark matter profile, we can hope to compare the dynamically derived constraints on ρ_0, r_0 with the scaling relations found from the data. In a separate article, we shall examine more general forms of halo dark matter distribution suggested by this dynamics [50].

If $\rho_D(r)$ and $\rho_{\mathrm{dm}}(r)$ are known we can use the hydrostatic equilibrium condition to figure out the temperature profile, $T(r)$. To do this, we need a boundary condition. Far from the galactic center, i.e. far from heating sources we expect isothermal conditions, which motivates $dT/dr = 0$ at large galactic distances, R_{gal}, which we take to be $50r_D$. Our numerical results are approximately independent of the particular value of R_{gal} chosen so long as $R_{\mathrm{gal}} \gg r_D$. To get an idea of the typical temperature profiles that we expect for spiral galaxies, we consider three examples: (a) a small-sized spiral galaxy with disk mass $m_D = 10^9 m_\odot$ and dark matter core radius $r_0 = 4$ kpc, (b) a medium-sized spiral galaxy ($\sim$ Milky Way) with disk mass $m_D = 10^{11}m_\odot$ and dark matter core radius $r_0 = 12$ kpc and (c) a large-sized spiral galaxy with disk mass $m_D = 10^{12}m_\odot$ and dark matter core radius $r_0 = 40$ kpc. In each case we take $\rho_0 = 10^2(m_\odot/\mathrm{pc}^2)/r_0$, consistent with results inferred from observations [41–43]. The results of numerically solving Eq. (9) with the boundary condition discussed above are shown in Fig. 1. The figure indicates that with a Burkert dark matter density profile the corresponding temperature profile derived from the hydrostatic equilibrium condition smoothly rises towards the central region of the galaxy, where it is roughly isothermal.

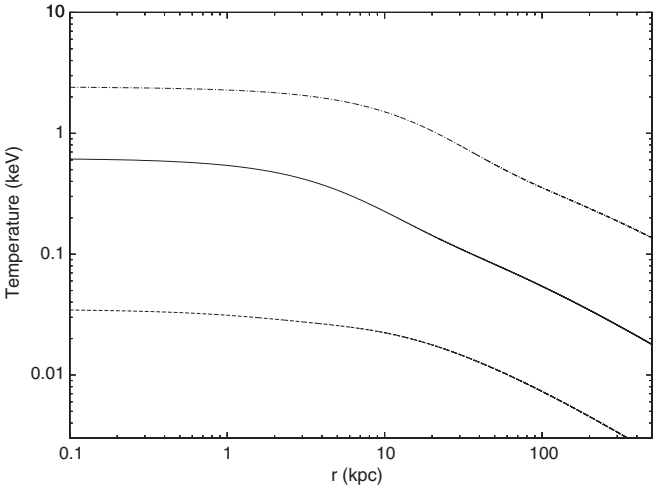

FIG. 1. The temperature profile of the mirror dark matter plasma in spiral galaxies for three examples: (a) a small-sized spiral galaxy with disk mass $m_D = 10^9 m_\odot$ and dark matter core radius $r_0 = 4$ kpc (dashed line), (b) a medium-sized spiral galaxy ($\sim$ Milky Way) with disk mass $m_D = 10^{11}m_\odot$ and dark matter core radius $r_0 = 12$ kpc (solid line) and (c) a large-sized spiral galaxy with disk mass $m_D = 10^{12}m_\odot$ and dark matter core radius $r_0 = 40$ kpc (dashed-dotted line). In each case we take $\rho_0 = 10^2(m_\odot/\mathrm{pc}^2)/r_0$.

IV. THE IONIZATION STATE OF THE HALO

For the temperature range of interest for spiral galaxies, typically 0.01 keV $\lesssim T \lesssim$ few keV, the plasma is kept ionized by e' collisions. Considering just the mirror helium component for now, the relevant processes are

$$e' + \mathrm{He}'^0 \rightarrow \mathrm{He}'^+ + e' + e', \qquad e' + \mathrm{He}'^+ \rightarrow \mathrm{He}'^{2+} + e' + e', \quad (15)$$

where He'^0, He'^+, He'^{++} denote the neutral mirror helium atom, singly charged mirror helium ion and doubly charged mirror helium ion. Since the Lagrangian describing the particle physics of the mirror particles is exactly analogous to the one describing the ordinary particles and forces, the cross section for the above processes is precisely the same as for the corresponding ordinary-particle process. The cross section for these processes is known to be reasonably well approximated by the Lotz formula [51],

$$\sigma_I = 4.5 \times 10^{-14}\left[\frac{\ln(E/I)}{EI/\mathrm{eV}^2}\right]\mathrm{cm}^2, \quad (16)$$

where $E \geq I$ is the energy of the incident e' and I is the ionization potential. For the first process in Eq. (15) $I = 24.6$ eV, while in the second process $I = 54.4$ eV. We denote the corresponding cross sections as σ_I^a and σ_I^b respectively.

Opposing ionization are the e' capture processes. The relevant processes for He' are

$$e' + \mathrm{He}'^+ \rightarrow \mathrm{He}'^0 + \gamma', \quad e' + \mathrm{He}'^{2+} \rightarrow \mathrm{He}'^+ + \gamma'. \quad (17)$$

The cross section for the capture processes can be approximated by a modified Kramers formula [52],

$$\sigma_C = \sum_n \frac{8\pi}{3\sqrt{3}} \frac{\alpha^5}{n^3} \frac{Z_{\rm eff}^4}{E_{e'} E_{\gamma'}}, \tag{18}$$

where $E_{\gamma'} = E_{e'} + \frac{Z_{\rm eff}^2 \alpha^2 m_e}{2n^2}$. For the applications to He$'$, H$'$ and also Fe$'$ ions that we will consider, $Z_{\rm eff} = (Z_C + Z_I)/2$, where Z_C is the charge of the nuclei and Z_I is the ionic charge before e' capture [52]. Thus, $Z_{\rm eff} \approx 1.5$ for the first process in Eq. (17), and $Z_{\rm eff} = 2$ for the second process. We denote the corresponding cross sections as σ_C^a and σ_C^b respectively.

The above processes dictate the number density of He$'^{2+}$ via

$$\frac{dn_{\rm He'^{2+}}}{dt} = n_{e'} n_{\rm He'^{+}} \langle \sigma_I^b v_{e'} \rangle - n_{e'} n_{\rm He'^{2+}} \langle \sigma_C^b v_{e'} \rangle, \tag{19}$$

where the brackets $\langle \ldots \rangle$ indicate the average over the e' velocity distribution taken as a Maxwell-Boltzman distribution,

$$\begin{aligned} \langle \sigma_I^b v_{e'} \rangle &\equiv 2\sqrt{\frac{2}{m_e \pi}} \left(\frac{1}{T}\right)^{3/2} \int_I^\infty \sigma_I^b e^{-E_{e'}/T} E_{e'} dE_{e'}, \\ \langle \sigma_C^b v_{e'} \rangle &\equiv 2\sqrt{\frac{2}{m_e \pi}} \left(\frac{1}{T}\right)^{3/2} \int_0^\infty \sigma_C^b e^{-E_{e'}/T} E_{e'} dE_{e'}. \end{aligned} \tag{20}$$

In a steady-state situation, we have $dn_{\rm He'^{2+}}/dt = 0$ and thus

$$R_2^{\rm He'} \equiv \frac{n_{\rm He'^{2+}}}{n_{\rm He'^{+}}} = \frac{\langle \sigma_I^b v_{e'} \rangle}{\langle \sigma_C^b v_{e'} \rangle}. \tag{21}$$

Similarly for the processes affecting $dn_{\rm He'^{0}}/dt$, and for the corresponding process for mirror hydrogen,

$$R_1^{\rm He'} \equiv \frac{n_{\rm He'^{+}}}{n_{\rm He'^{0}}} = \frac{\langle \sigma_I^a v_{e'} \rangle}{\langle \sigma_C^a v_{e'} \rangle}, \quad R_1^{\rm H'} \equiv \frac{n_{\rm H'^{+}}}{n_{\rm H'^{0}}} = \frac{\langle \sigma_I v_{e'} \rangle}{\langle \sigma_C v_{e'} \rangle}, \tag{22}$$

where σ_I and σ_C are the relevant cross sections for the mirror hydrogen process. The H$'$ ionization cross section is given by Eq. (16) with $I = 13.6$ eV, while the capture cross section is given by Eq. (18) with $Z_{\rm eff} = 1$.

With these definitions we can determine the number density of each component as a function of another component, which we choose to be $n_{\rm He'} = n_{\rm He'^{0}} + n_{\rm He'^{+}} + n_{\rm He'^{2+}}$:

$$\begin{aligned} n_{\rm He'^{2+}} &= \left(\frac{R_1^{\rm He'} R_2^{\rm He'}}{1 + R_1^{\rm He'} + R_1^{\rm He'} R_2^{\rm He'}}\right) n_{\rm He'}, \\ n_{\rm He'^{+}} &= \left(\frac{R_1^{\rm He'}}{1 + R_1^{\rm He'} + R_1^{\rm He'} R_2^{\rm He'}}\right) n_{\rm He'}, \\ n_{\rm He'^{0}} &= n_{\rm He'} - n_{\rm He'^{+}} - n_{\rm He'^{2+}}, \qquad n_{\rm H'}^{+} = \left(\frac{R_1^{\rm H'}}{1 + R_1^{\rm H'}}\right) f n_{\rm He'}, \\ n_{\rm H'^{0}} &= f n_{\rm He'} - n_{\rm H'^{+}}, \qquad n_{e'} = 2n_{\rm He'^{2+}} + n_{\rm He'^{+}} + n_{\rm H'^{+}}, \\ n_T &= (1+f) n_{\rm He'} + n_{e'}, \end{aligned} \tag{23}$$

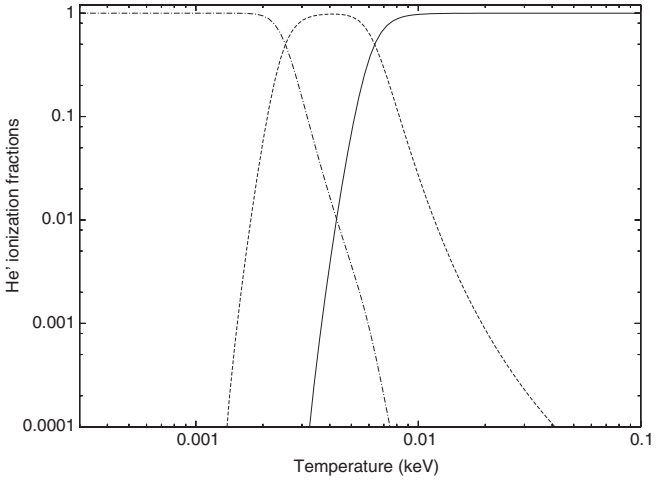

FIG. 2. The He$'$ ionization fractions, as a function of the local halo temperature, T. Shown are $F_0^{\rm He'} \equiv n_{\rm He'^{0}}/n_{\rm He'}$ (dashed-dotted line), $F_1^{\rm He'} \equiv n_{\rm He'^{+}}/n_{\rm He'}$ (dashed line) and $F_2^{\rm He'} \equiv n_{\rm He'^{2+}}/n_{\rm He'}$ (solid line).

where $f \equiv n_{\rm H'}/n_{\rm He'}$ and n_T is the total particle number density. The fraction, f, can be related to the He$'$ mass fraction,

$$\xi_{\rm He'} = \frac{1}{1 + f/4}. \tag{24}$$

Unless otherwise stated, we take $f = 0.4$ in our numerical work (which, as we already discussed at the beginning of the previous section, is suggested from early Universe cosmology). The quantities $R_{1,2}^{\rm He'}$ and $R_1^{\rm H'}$ depend only on the temperature. It is straightforward to compute the He$'$ ionization fractions, $F_0^{\rm He'} \equiv n_{\rm He'^{0}}/n_{\rm He'}$, $F_1^{\rm He'} \equiv n_{\rm He'^{+}}/n_{\rm He'}$, $F_2^{\rm He'} \equiv n_{\rm He'^{2+}}/n_{\rm He'}$, and also the H$'$ ionization fractions, $F_0^{\rm H'} \equiv n_{\rm H'^{0}}/n_{\rm H'}$, $F_1^{\rm H'} \equiv n_{\rm H'^{+}}/n_{\rm H'}$. We show these results in Fig. 2 for He$'$ and Fig. 3 for H$'$. Figure 2 indicates that He$'$

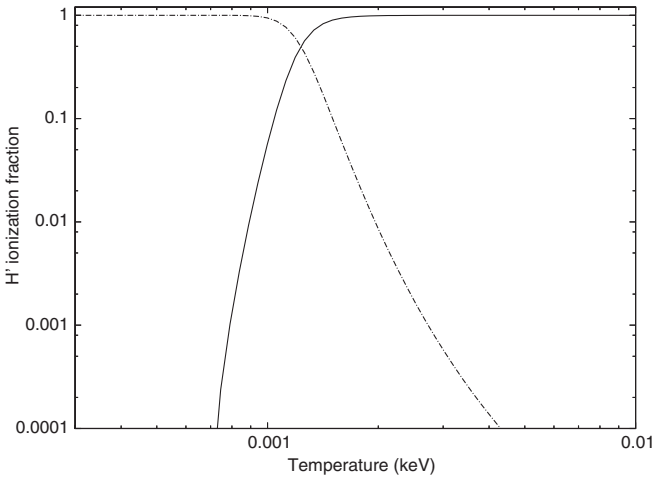

FIG. 3. The H$'$ ionization fractions, as a function of the local halo temperature, T. Shown are $F_0^{\rm H'} \equiv n_{\rm H'^{0}}/n_{\rm H'}$ (dashed-dotted line) and $F_1^{\rm H'} \equiv n_{\rm H'^{+}}/n_{\rm H'}$ (solid line).

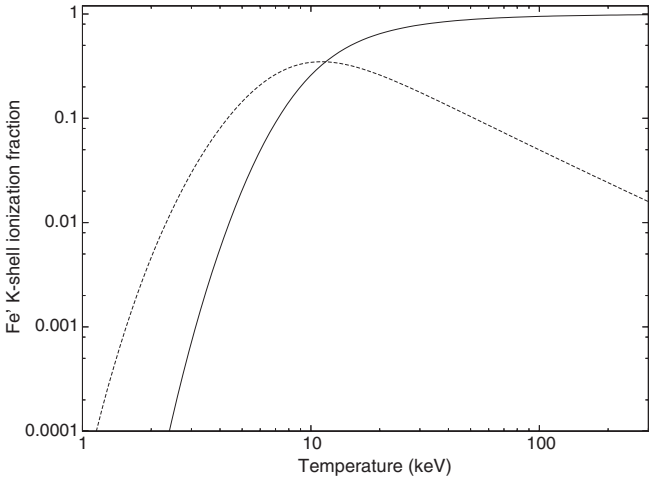

FIG. 4. The Fe′ ionization fractions $F_1^{\mathrm{Fe}'} \equiv n_{\mathrm{Fe}'^*}/n_{\mathrm{Fe}'}$ (dashed line), $F_2^{\mathrm{Fe}'} \equiv n_{\mathrm{Fe}'^{**}}/n_{\mathrm{Fe}'}$ (solid line) as a function of the local halo temperature, T.

is nearly fully ionized for $T \gtrsim 10$ eV. This is substantially below the $I = 54.4$ eV ionization energy of He'^+, which occurs because the capture cross section is several orders of magnitude smaller than the ionization cross section. Qualitatively similar results also arise for H′.

In addition to the pure H′, He′ halo, we will consider a small metal component, which we take as Fe′ with a total number density, $n_{\mathrm{Fe}'}$ [the Fe′ component was presumably formed in mirror stars at an early epoch; see earlier discussion Eq. (8)]. We denote the number density of completely ionized Fe′ as $n_{\mathrm{Fe}'^{**}}$ and Fe′ with one K-shell e' as $n_{\mathrm{Fe}'^*}$. The ionization energy of the bound mirror electron in Fe'^* is 9.3 keV and if both K-shell mirror electrons are present, the binding energy is 8.8 keV [53]. In Fig. 4 we show the computed ionization fractions $F_1^{\mathrm{Fe}'} \equiv n_{\mathrm{Fe}'^*}/n_{\mathrm{Fe}'}$ and $F_2^{\mathrm{Fe}'} \equiv n_{\mathrm{Fe}'^{**}}/n_{\mathrm{Fe}'}$ versus temperature. Figure 4 indicates that Fe′ is nearly fully ionized until the temperature drops below around 20 keV i.e. somewhat above the ionization energy of the K-shell bound mirror electrons. (This occurs because the Fe'^* capture cross section is somewhat larger than the ionization cross section.) For temperatures below around 2 keV, greater than 99 percent of the Fe′ ions typically have both atomic K-shell states filled.

V. HALO ENERGETICS AND SCALING RELATIONS

Studies of spiral galaxies have found that the baryonic parameters m_D, r_D, L_r satisfy two approximate relations. One of these relations was given in the previous section, Eq. (13); the other relates the r^*-band luminosity, L_r to m_D (see e.g. Ref. [54] and references therein),

$$\frac{m_D}{10^{11} m_\odot} \approx \left(\frac{L_r}{L_r^{\mathrm{MW}}}\right)^{1.3}, \tag{25}$$

where $L_r^{\mathrm{MW}} \approx 2 \times 10^{10} L_\odot$ is the r^*-band luminosity of the Milky Way. With these relations, the baryonic parameters of spirals are (roughly) specified by a single parameter which can be taken as one of m_D, r_D or L_r. If we assume that the dark matter is distributed via the Burkert profile, Eq. (14), then we have two further parameters: ρ_0 and r_0. Our aim is to derive constraints on these two dark matter parameters from dynamical considerations. The derived constraints can then be compared with "empirical" relations derived from observations of rotation curves in spiral galaxies [3,41–43,48,54,55],

$$\begin{aligned} \log\left(\frac{\rho_0 r_0}{m_\odot\ \mathrm{pc}^{-2}}\right) &\simeq 2.2 \pm 0.25, \\ \frac{L_r}{1.2 \times 10^{10} L_\odot} &\simeq \frac{\left(\frac{m_h}{3\times 10^{11} m_\odot}\right)^{2.65}}{1 + \left(\frac{m_h}{3\times 10^{11} m_\odot}\right)^{2.00}}, \\ \log\left(\frac{r_0}{\mathrm{kpc}}\right) &\simeq 0.66 + 0.58 \log\left(\frac{m_h}{10^{11} m_\odot}\right), \end{aligned} \tag{26}$$

where m_h is the halo mass. Spiral galaxies typically have halos in the mass range $10^{11} m_\odot \lesssim m_h \lesssim 10^{13} m_\odot$ and baryonic mass in the range $10^9 m_\odot \lesssim m_D \lesssim 10^{12} m_\odot$.

As discussed in Refs. [33,38] and reviewed in Sec. II, the energy lost in the halo due to dissipative processes might be replaced by supernova energy transported to the halo via mirror photons.[5] For this idea to work out, the halo must evolve to a state such that the energy being absorbed in each volume element must equate to the energy being radiated from the same volume element. Thus, we have a dynamical condition,

$$\frac{d^2 E_{\mathrm{in}}}{dt dV} = \frac{d^2 E_{\mathrm{out}}}{dt dV}. \tag{27}$$

In the following, we derive approximate formulas for the left- and right-hand sides of the above equation. Subsequently we solve the derived equations numerically. We will show that the above dynamical condition can be approximately satisfied with the Burkert dark matter profile provided that ρ_0 and r_0 satisfy certain relations. These relations are then compared with the "empirical" relations obtained from galactic rotation curve (and other) data, discussed above.

The region around a single supernova will be a source of a huge flux of mirror photons with total integrated luminosity of around 10^{53} erg, provided a photon-mirror photon kinetic mixing with a strength of $\epsilon \sim 10^{-9}$ exists. We define the total (time) average mirror photon luminosity due to ordinary core-collapse supernovae by

[5]One can check that the energy transport due to other processes, such as conduction, is negligible in comparison to radiation. This is, of course, due to the fact that the mirror photons have a much longer scattering length than mirror electrons.

$$L'_{\rm SN} \equiv R_{\rm SN} f_{\rm SN} \langle E_{\rm SN} \rangle, \tag{28}$$

where $R_{\rm SN}$ is the galactic supernova rate, $f_{\rm SN}$ is the fraction of supernovae energy emitted by mirror particles e', $\bar{e}'$, γ', and $\langle E_{\rm SN} \rangle$ is the average total energy emitted per supernova. The quantity $L'_{\rm SN}$ obviously depends on the particular galaxy concerned. For the Milky Way galaxy, we have

$$L'^{\rm MW}_{\rm SN} \approx \left(\frac{R^{\rm MW}_{\rm SN}}{0.03\ {\rm yr}^{-1}}\right)\left(\frac{f_{\rm SN}}{0.5}\right)\left(\frac{\langle E_{\rm SN}\rangle}{3\times 10^{53}\ {\rm erg}}\right) 1.4\times 10^{44}\ {\rm erg/s}. \tag{29}$$

To proceed further we will need to parametrize the γ' supernova energy spectrum averaged over all ordinary supernova. We assume that the peak of this (averaged) γ' energy spectrum occurs at energies somewhat greater than the K-shell e' atomic binding energy of Fe′, ∼9 keV. In this case only the low-energy part of the spectrum can heat the halo. We parametrize this energy spectrum via a power law,

$$E_{\gamma'}\frac{dN_{\gamma'}}{dE_{\gamma'}} = \left(\frac{1+c_1}{E_c}\right)\left(\frac{E_{\gamma'}}{E_c}\right)^{c_1} f_{\rm SN} E_{\rm SN} \equiv \kappa (E_{\gamma'})^{c_1}. \tag{30}$$

This spectrum has been normalized such that

$$\int_0^{E_c} E_{\gamma'}\frac{dN_{\gamma'}}{dE_{\gamma'}} dE_{\gamma'} = f_{\rm SN} E_{\rm SN}. \tag{31}$$

We will consider $1 \le c_1 \le 3$ in our numerical work ($c_1 = 2$ corresponds to a thermal spectrum). Although the spectrum would not be expected to be a power law for sufficiently high energies, such details will be unimportant since the halo is optically thin at energies $E'_\gamma \gtrsim 30$ keV.

Observations indicate that the supernova rate scales with galactic B-band luminosity, L_B, via $R_{\rm SN} \propto (L_B)^{0.73}$, with an uncertainty in the exponent around 0.1 [56]. With the above definitions, we find that for $f_{\rm SN} \approx 0.5$ (i.e. for $\epsilon \sim 10^{-9}$)

$$\kappa R_{\rm SN} \approx \frac{1+c_1}{(E_c)^{1+c_1}}\left(\frac{L_B}{L^{\rm MW}_B}\right)^{0.73} L'^{\rm MW}_{\rm SN}, \tag{32}$$

where $L^{\rm MW}_B \approx 2\times 10^{10} L_\odot$ is the reference B-band luminosity for the Milky Way. Although there is substantial uncertainty in $L'^{\rm MW}_{\rm SN}$, possibly as large as an order of magnitude, the galactic scaling behavior of $\kappa R_{\rm SN}$ should be more certain.

The energy spectrum of γ' from a single supernova source is given in Eq. (30). The supernovae are distributed throughout the disk. We wish to figure out the (time) average γ' flux at a point P a distance r from the galactic center, from all supernova sources. We assume that the supernova distribution traces the baryonic mass density [Eq. (12)]. It then follows that the contribution to the γ' energy flux at P originating from a volume element, $dV' = 2\pi r'^2 d\cos\theta dr'$, at a point Q is

$$\frac{d^2F(r)}{dE_{\gamma'}dV'} = \frac{\kappa (E_{\gamma'})^{c_1} R_{\rm SN} e^{-\tau}}{4\pi {\rm d}^2}\frac{\rho_D}{m_D}, \tag{33}$$

where κ is defined in Eq. (30), ${\rm d} = \sqrt{r^2 + r'^2 - 2rr'\cos\theta}$ is the distance of the source Q to the point P and τ is the optical depth along that path. Summing over all contributions we find that the total differential energy flux is given by

$$\frac{dF(r)}{dE_{\gamma'}} = \frac{\kappa (E_{\gamma'})^{c_1} R_{\rm SN}}{m_D}\int_0^\infty \int_{-1}^1 \frac{\rho_D e^{-\tau} r'^2}{2{\rm d}^2} d\cos\theta dr'. \tag{34}$$

The optical depth τ is given by

$$\tau = \int_0^{\rm d} \sum_i n_i(r_1)\sigma_i dy. \tag{35}$$

The relevant geometry is shown in Fig. 5, and we have

$$r_1 = \sqrt{y^2 + r'^2 - 2r'y\cos\psi}, \qquad \cos\psi = \frac{{\rm d}^2 + r'^2 - r^2}{2r'{\rm d}}. \tag{36}$$

The flux of supernova γ' at a particular point P will deposit an energy per unit volume per unit time of

$$\frac{d^3E_{\rm in}}{dE_{\gamma'}dtdV} = \frac{dF}{dE_{\gamma'}}\sum_i n_i(r)\sigma_i. \tag{37}$$

Thus to calculate the heating at a particular point in the halo we need to determine the cross section and number densities of the various components in the halo [denumerated by i in Eqs. (35) and (37)]. The supernova γ' are assumed to have relatively high energies, so that the optical depth is dominated by scattering of γ' off bound atomic e'. This is possible because heavy elements, such as Si′ and Fe′, are not completely ionized but have their atomic inner shells filled. If the flux of supernova γ' are falling below 10 keV, then the interactions with K-shell Fe′ mirror electrons are likely to be the most important (see discussion in Sec. II). The total photoelectric cross section is given approximately by Eq. (4) and the Fe′ number density is given by $n_{\rm Fe'} = n_{\rm He'}(1+\frac{f}{4})(\frac{m_{\rm He}}{m_{\rm Fe}})(\frac{\xi_{\rm Fe'}}{1-\xi_{\rm Fe'}})$. (Also needed are the Fe′ ionization fractions which can be computed as per Sec. IV.)

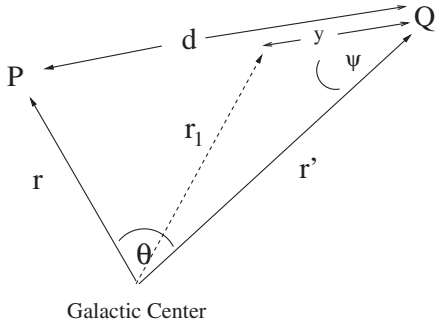

FIG. 5. The geometry. Mirror photons travel a distance d from a supernova source at point Q, to heat the halo at a point P.

Having discussed the heating rate at the point P in the halo, we now turn our attention to the cooling rate at the same point. The cooling rate is expected to have contributions from three sources: thermal bremsstrahlung, line emission and recombination. We first consider the bremsstrahlung component and comment on the line emission and recombination contributions in a moment.

The rate at which bremsstrahlung energy is radiated per unit volume, per unit time is [40]

$$\frac{d^2W}{dtdV} = \frac{16\alpha^3}{3m_e}\left(\frac{2\pi T}{3m_e}\right)^{1/2}\sum_j [Z_j^2 n_j n_{e'} \bar{g}_B], \qquad (38)$$

where the index j runs over the mirror ions in the plasma (of charge Z_j) and $\bar{g}_B$ is the frequency average of the velocity averaged Gaunt factor for free-free emission. We take $\bar{g}_B = 1.2$, which, as reviewed in Ref. [40], should be accurate to within about 20%.

In principle the energy radiated at a point P can have important contributions from line emission and recombination in addition to bremsstrahlung. Such processes would depend on the detailed chemical composition of the halo. However these processes may not be as important as naive first thoughts suggest. The energy of the radiated mirror photons from line emission and recombination is typically close to the halo temperature, T. But the halo is generally expected to be optically thick to mirror photons of these energies (rough estimates indicate). Thus, the capacity of these processes to directly cool the halo is expected to be greatly diminished. Bremsstrahlung, on the other hand, generally produces mirror photons of lower energy. The energy spectrum of bremsstrahlung is flat for $E_{\gamma'} \ll T$. and reduces towards zero for increasing T like $\sim \exp(-E_{\gamma'}/T)$ (see e.g. Ref. [40]). We therefore expect that the bremsstrahlung process will cool the halo much more efficiently. As a rough approximation, we set $\frac{d^2E_{\rm out}}{dtdV} = \epsilon_f \frac{d^2W}{dtdV}$, where ϵ_f is an efficiency factor which we set to unity in our numerical work. If the bremsstrahlung process is the dominant cooling mechanism then $\frac{dE_{\rm out}}{dtdV} \propto \sqrt{T}$, that is, an increasing function of T. This might explain why the system evolves until $dE_{\rm in} = dE_{\rm out}$. If a region had $dE_{\rm in} > dE_{\rm out}$ then this will make T higher in that region which also increases $dE_{\rm out}$ until $dE_{\rm in} = dE_{\rm out}$. Similarly if $dE_{\rm in} < dE_{\rm out}$ then this will make T smaller which decreases $dE_{\rm out}$ until $dE_{\rm in} = dE_{\rm out}$. It therefore seems plausible that the system will evolve until the dynamical condition, Eq. (27), is satisfied everywhere.[6]

[6]Naturally the system is a complicated one and other feedback mechanisms can also be important. For instance, a mismatch of $dE_{\rm in}$ and $dE_{\rm out}$ can also cause an expansion or contraction of the halo, which in turn can affect the ordinary star formation rate and thereby readjust $dE_{\rm in}$. Such a feedback mechanism may also help regulate the star formation rate as suggested by observations (see Ref. [57] and references therein for relevant discussions).

We are now ready to start solving the equations. The philosophy is that if the dark matter density can be parametrized by the form given in Eq. (14) then ρ_0 and r_0 can be determined by demanding that $\frac{d^2E_{\rm in}}{dtdV} \simeq \frac{d^2E_{\rm out}}{dtdV}$ for each volume element. To quantify how well $dE_{\rm in}$ and $dE_{\rm out}$ match, we introduce the quantity Δ,

$$\Delta(r_0, \rho_0) \equiv \frac{1}{10r_D}\int_{r_D}^{11r_D}\left|1 - \frac{\frac{d^2E_{\rm in}}{dtdV}}{\frac{d^2E_{\rm out}}{dtdV}}\right| dr. \qquad (39)$$

The quantity Δ can be computed numerically via a FORTRAN code. The adopted procedure is to input the dark matter density profile and the baryonic density and work out the temperature profile using the hydrostatic equilibrium condition as described in Sec. III. Once the temperature profile is known, one can work out the ionization state of the halo via the equations described in Sec. IV. Armed with this information, one can proceed to work out Eqs. (34), (37), and (38), the latter we equate to $\frac{d^2E_{\rm out}}{dtdV}$. The end result is the trivial integration (39) to obtain Δ as a function of the input parameters ρ_0, r_0 as well as baryonic parameter, m_D [r_D and L are obtained from Eqs. (13) and (25)].

We start by examining how compatible the Burkert dark matter profile is with the $\frac{d^2E_{\rm in}}{dtdV} = \frac{d^2E_{\rm out}}{dtdV}$ condition. We define $\Delta^a_{\rm min}(r_0)$ as the quantity $\Delta(r_0, \rho_0)$ minimized with respect to variations in ρ_0. Similarly, $\Delta^b_{\rm min}(\rho_0)$ is defined by minimizing $\Delta(r_0, \rho_0)$ with respect to variations in r_0. In Fig. 6(a) we plot $\Delta^a_{\rm min}(r_0)$ versus r_0 and in Fig. 6(b) we plot $\Delta^b_{\rm min}(\rho_0)$ versus ρ_0. These figures are for an example point with $m_D = 10^{11}m_\odot$ and reference parameters $f \equiv n_{\rm H'}/n_{\rm He'} = 0.4$, $\xi_{\rm Fe'} = 0.02$, $L_{\rm SN}^{\prime\rm MW} = 2 \times 10^{45}$ erg/s, $E_c = 50$ keV.

The figures show that Δ has a minimum value of around 0.1. That is, $\frac{d^2E_{\rm in}}{dtdV} = \frac{d^2E_{\rm out}}{dtdV}$ to within around 10%. In Fig. 6(c), we plot $\frac{d^2E_{\rm in}}{dtdV} / \frac{d^2E_{\rm out}}{dtdV}$ (evaluated at the ρ_0, r_0 values which minimize Δ) versus the galactic radius r/r_D. This is done for the same example as Figs. 6(a) and 6(b). This figure demonstrates that the Burkert profile does a very good job of minimizing Δ with only small deviations near the galactic center, which are unlikely to be important since ordinary baryons dominate the mass density there (see e.g. Ref. [3] and references therein). We have found that varying m_D and variations in the other parameters give similar results. This demonstrates that the Burkert profile is (roughly) compatible with the condition (27). Furthermore, for each value of m_D we can estimate the values of r_0 and ρ_0 by minimizing Δ, as we have just done for the particular example with $m_D = 10^{11}m_\odot$. This leads to relations connecting the baryonic parameters (m_D, r_D, L) with the dark matter parameters, ρ_0, r_0. Although we expect to derive only two independent relations, we explore our results by considering three plots. In Fig. 7(a) we plot L versus r_0, in Fig. 7(b) we plot ρ_0 versus m_D and in Fig. 7(c) we plot $\rho_0 r_0$ versus L. In each case we consider various values of

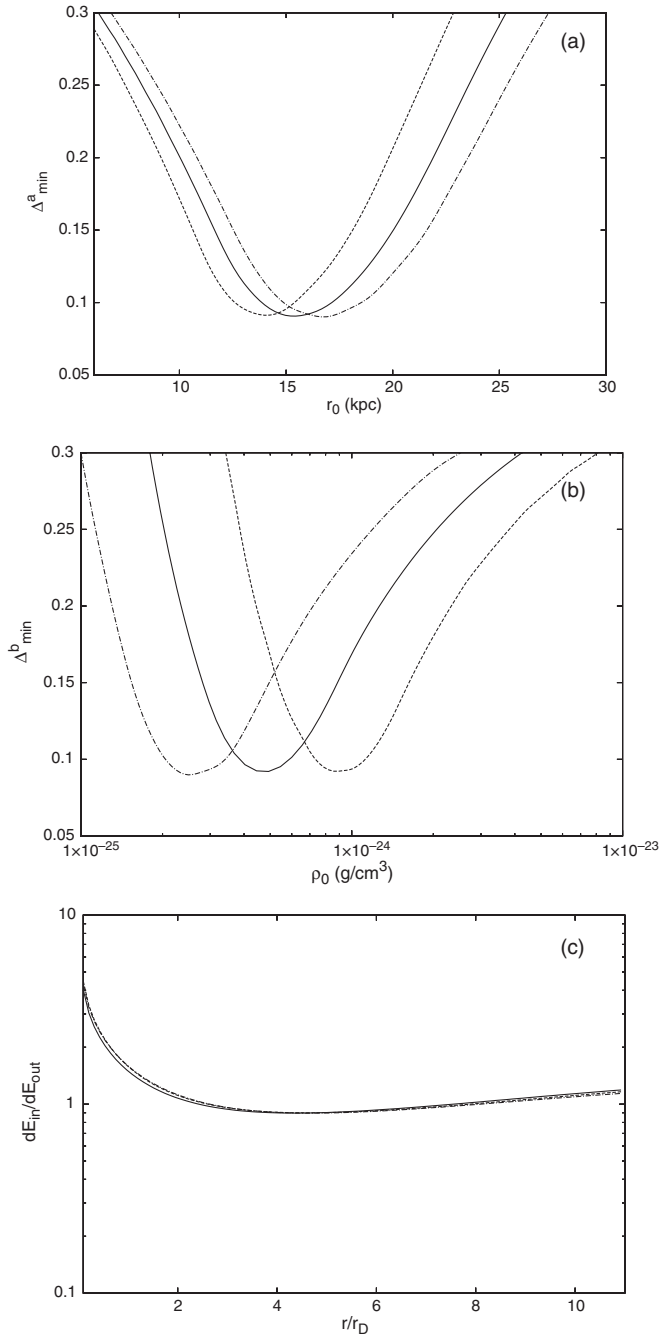

FIG. 6. (a) $\Delta^a_{\rm min}$ (defined in text) versus the core radius, r_0 for $m_D = 10^{11} m_\odot$. Plotted are various values of c_1 which parametrize the hardness of the mirror photon supernova spectrum: $c_1 = 1$ (dashed line), $c_1 = 2$ (solid line) and $c_1 = 3$ (dashed-dotted line). (b) Same as for Fig. 6(a), except $\Delta^b_{\rm min}$ is plotted versus ρ_0. (c) $\frac{d^2E_{\rm in}}{dtdV} / \frac{d^2E_{\rm out}}{dtdV}$ versus r/r_D for the same example as Figs. 6(a) and 6(b). The values of r_0, ρ_0 taken are the ones which minimize Δ. Three curves (almost indistinguishable) correspond to the same three c_1 values of Figs. 6(a) and 6(b).

c_1 which, we recall, parametrizes the hardness of the supernova γ' spectrum. Other parameters fixed are $f \equiv n_{H'}/n_{He'} = 0.4$, $\xi_{Fe'} = 0.02$. The quantity $\kappa R_{\rm SN}$ is given in Eq. (32) with $E_c = 50$ keV and $L'^{\rm MW}_{\rm SN} = 2 \times 10^{45}$ erg/s.

The figures demonstrate that the derived relations for ρ_0, r_0 are compatible with the rough "empirical" scaling relations given in Eq. (26).[7] The level of agreement seems to be very nontrivial. The only parameter adjusted was $L'^{\rm MW}_{\rm SN}$ which was set so that $\rho_0 r_0$ had a value $\sim 10^2 m_\odot/{\rm pc}^2$ for $m_D = 10^{11} m_\odot$, $c_1 = 2$.

To check the robustness of these results with respect to reasonable parameter variations we have varied $\xi_{Fe'}$, $L'^{\rm MW}_{\rm SN}$. (Note that changing E_c has the same effect as changing $L'^{\rm MW}_{\rm SN}$ and is therefore not considered.) In Fig. 8 (Fig. 9) we show the effect of varying $L'^{\rm MW}_{\rm SN}$ ($\xi_{Fe'}$), with the other parameters unchanged. These figures demonstrate that the variation of each of these parameters by an order of magnitude around our reference values does *not* greatly modify the L versus r_0 relation [Fig. 7(a)]. They also show that $\rho_0 r_0$ is still constant but the value of the constant is modified somewhat. We have also found that the above conclusions hold also when $f \equiv n_{H'}/n_{He'}$ is changed. Thus, the scaling properties demonstrated in Figs. 7(a)–7(c) remain valid even when parameters are varied. Figures 7–9 indicate that the effect of varying c_1, $\xi_{Fe'}$ and $L'^{\rm MW}_{\rm SN}$ on $\rho_0 r_0$ can be roughly approximated by

$$\rho_0 r_0 \simeq \left[\frac{\xi_{Fe'}}{0.02}\right]^{0.7} \left[\frac{L'^{\rm MW}_{\rm SN}}{2 \times 10^{45}\ {\rm erg/s}}\right]^{0.7} \left[\frac{2}{c_1}\right] 10^2 m_\odot/{\rm pc}^2. \tag{40}$$

On the other hand the L versus r_0 relation is remarkably insensitive to variations of the parameters. Instead of fixing the baryonic parameters via the relations (13) and (25), we can consider independent variations of m_D, L and r_D. In doing so, we find that r_0 is mainly set by the parameter r_D. That is, it is primarily the disk scale length that sets the scale for the dark matter core radius. This suggests that the primary relation for r_0 is one in terms of r_D (not L). By fixing the baryonic parameters as per Eqs. (13) and (25) and minimizing Δ we obtain the approximate numerical result

$$r_0 \approx 3.0 \left(\frac{r_D}{\rm kpc}\right)^{1.1} {\rm kpc}. \tag{41}$$

As with our other results, this is valid over the considered baryonic mass range of spirals $10^9 m_\odot \lesssim m_D \lesssim 10^{12} m_\odot$, and we have assumed the Burkert profile.

These results are all very interesting, and—among other things—support the premise that kinetic mixing is likely close to $\epsilon = 10^{-9}$. Such a value has already been identified as a region of interest from the analysis [26] of direct detection experiments, such as DAMA [27]. The latter can be explained with $\epsilon\sqrt{\xi_{Fe'}} \approx 2 \times 10^{-10}$. Observe that since $L'^{\rm MW}_{\rm SN} \propto \epsilon^2$ [Eq. (3)], Eq. (40) suggests

$$\rho_0 r_0 \sim \left[\frac{\epsilon\sqrt{\xi_{Fe'}}}{5 \times 10^{-10}}\right]^{1.4} 10^2 m_\odot/{\rm pc}^2. \tag{42}$$

[7]We have neglected any possible scaling difference between the galactic r^* band luminosity, L_r, and B-band luminosity, L_B.

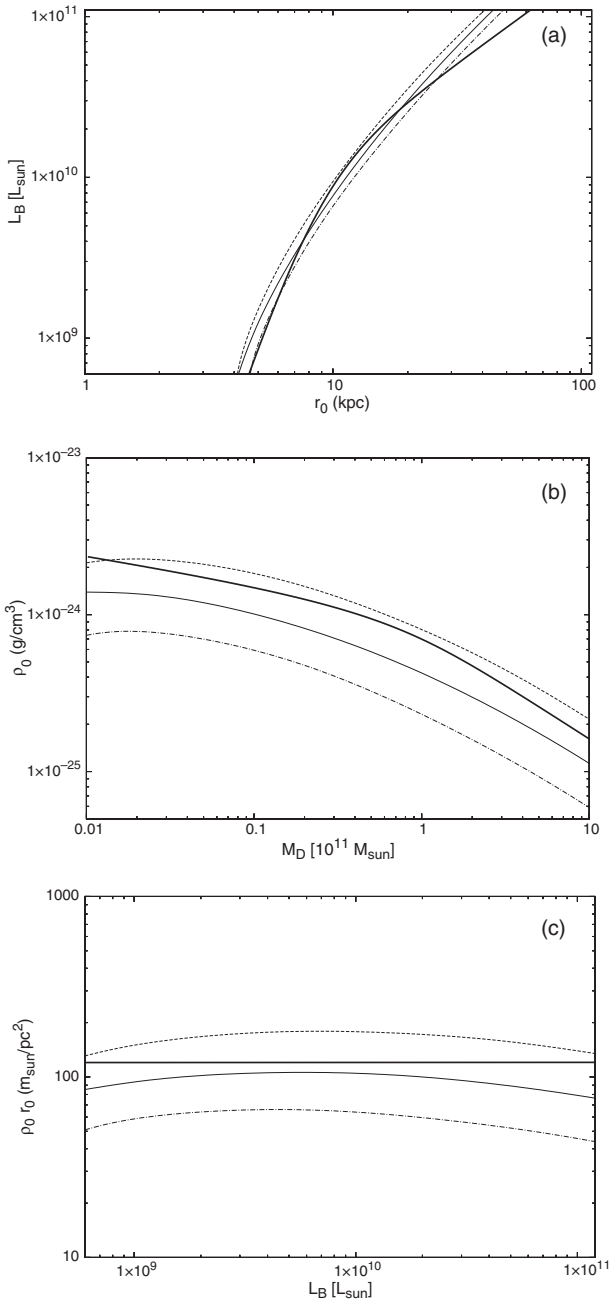

FIG. 7. (a) Derived galaxy luminosity versus core radius r_0 for various values of c_1 which parametrize the hardness of the supernova mirror photon spectrum. Plotted are $c_1 = 1$ (dashed line), $c_1 = 2$ (solid line) and $c_1 = 3$ (dashed-dotted line). Also shown (thick solid line) is the corresponding empirical galactic scaling relation obtained from Eq. (26). (b) Derived dark matter central density, ρ_0, versus baryonic mass, m_D, for various values of c_1. Plotted are $c_1 = 1$ (dashed line), $c_1 = 2$ (solid line) and $c_1 = 3$ (dashed-dotted line). Also shown (thick solid line) is the corresponding empirical galactic scaling relation obtained from Eqs. (25) and (26). (c) Derived $\rho_0 r_0$ as a function of galactic luminosity L_B for various values of c_1. Plotted are $c_1 = 1$ (dashed line), $c_1 = 2$ (solid line) and $c_1 = 3$ (dashed-dotted line). Also shown is $\rho_0 r_0 = 120 m_\odot/\mathrm{pc}^2$, close to the central value of the "empirical" relation (26) (thick solid line).

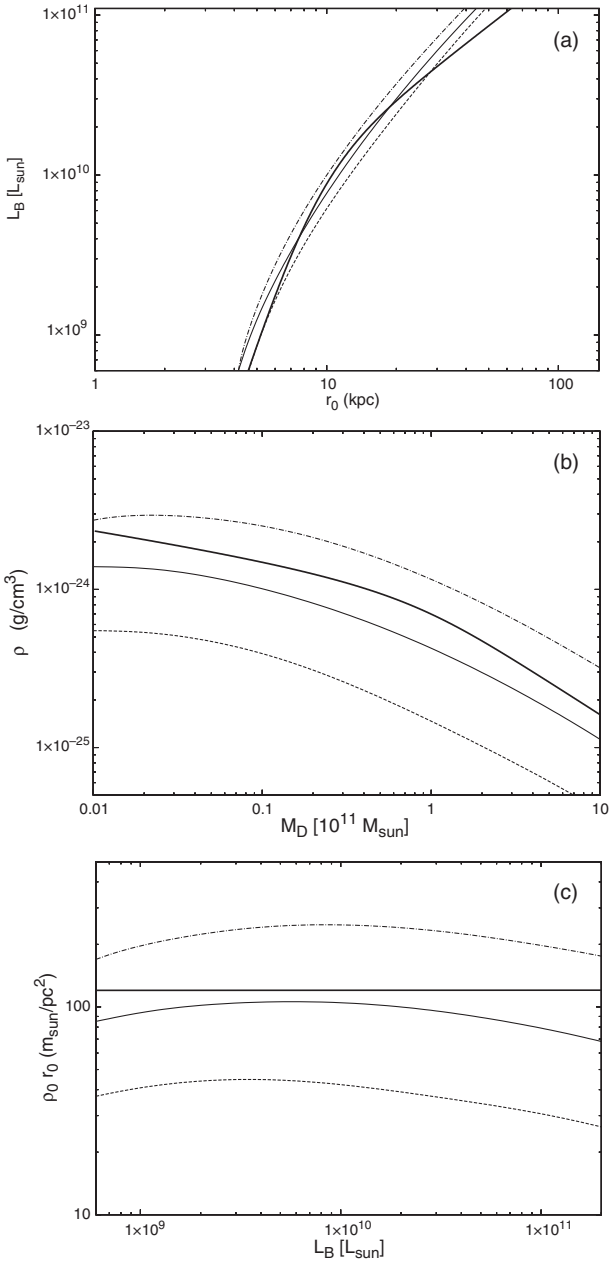

FIG. 8. (a) Derived galaxy luminosity versus core radius r_0 for $c_1 = 2$ and various values of $L_{\mathrm{SN}}^{\prime\mathrm{MW}}$. Plotted are $L_{\mathrm{SN}}^{\prime\mathrm{MW}} = 0.7 \times 10^{45}$ erg/s (dashed line), $L_{\mathrm{SN}}^{\prime\mathrm{MW}} = 2.0 \times 10^{45}$ erg/s (solid line) and $L_{\mathrm{SN}}^{\prime\mathrm{MW}} = 6.0 \times 10^{45}$ erg/s (dashed-dotted line). Also shown (thick solid line) is the corresponding empirical galactic scaling relation obtained from Eq. (26). (b) Derived dark matter density, ρ_0, versus baryonic mass, m_D, for $c_1 = 2$ and various values of $L_{\mathrm{SN}}^{\prime\mathrm{MW}}$: $L_{\mathrm{SN}}^{\prime\mathrm{MW}} = 0.7 \times 10^{45}$ erg/s (dashed line), $L_{\mathrm{SN}}^{\prime\mathrm{MW}} = 2.0 \times 10^{45}$ erg/s (solid line) and $L_{\mathrm{SN}}^{\prime\mathrm{MW}} = 6.0 \times 10^{45}$ erg/s (dashed-dotted line). Also shown (thick solid line) is the corresponding empirical galactic scaling relation obtained from Eqs. (25) and (26). (c) Derived $\rho_0 r_0$ as a function of galactic luminosity, L_B, for $c_1 = 2$ and various values of $L_{\mathrm{SN}}^{\prime\mathrm{MW}}$. Plotted are $L_{\mathrm{SN}}^{\prime\mathrm{MW}} = 0.7 \times 10^{45}$ erg/s (dashed line), $L_{\mathrm{SN}}^{\prime\mathrm{MW}} = 2.0 \times 10^{45}$ erg/s (solid line) and $L_{\mathrm{SN}}^{\prime\mathrm{MW}} = 6.0 \times 10^{45}$ erg/s (dashed-dotted line). Also shown is $\rho_0 r_0 = 120 m_\odot/\mathrm{pc}^2$, close to the central value of the "empirical" relation (26) (thick solid line).

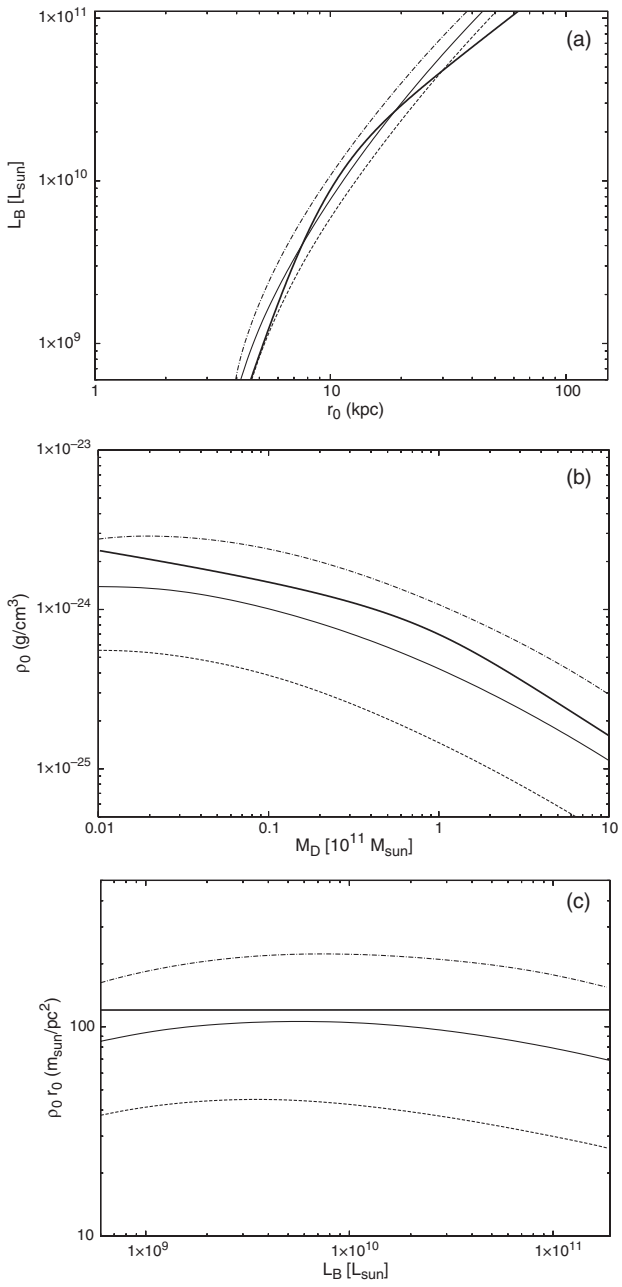

FIG. 9. (a) Derived galaxy luminosity versus core radius r_0 for $c_1 = 2$ and various values of $\xi_{Fe'}$. Plotted are $\xi_{Fe'} = 0.007$ (dashed line), $\xi_{Fe'} = 0.02$ (solid line) and $\xi_{Fe'} = 0.06$ (dashed-dotted line). Also shown (thick solid line) is the corresponding empirical galactic scaling relation obtained from Eq. (26). (b) Derived dark matter central density, ρ_0, versus baryonic mass, m_D, for $c_1 = 2$ and various values of $\xi_{Fe'}$. Plotted are $\xi_{Fe'} = 0.007$ (dashed line), $\xi_{Fe'} = 0.02$ (solid line) and $\xi_{Fe'} = 0.06$ (dashed-dotted line). Also shown (thick solid line) is the corresponding empirical galactic scaling relation obtained from Eqs. (25) and (26). (c) Derived $\rho_0 r_0$ as a function of galactic luminosity, L_B, for $c_1 = 2$ and various values of $\xi_{Fe'}$. Plotted are $\xi_{Fe'} = 0.007$ (dashed line), $\xi_{Fe'} = 0.02$ (solid line) and $\xi_{Fe'} = 0.06$ (dashed-dotted line). Also shown is $\rho_0 r_0 = 120 m_\odot/\mathrm{pc}^2$, close to the central value of the "empirical" relation (26) (thick solid line).

This demonstrates the compatibility of the galactic scaling relations with results from the direct detection experiments.

VI. DWARF SPHEROIDAL GALAXIES

The results of the previous section are very encouraging. One might be tempted to investigate other classes of galaxies, i.e. galaxies beyond spirals, and inquire if they are also compatible within this dissipative dark matter picture. An interesting class of galaxies is the dwarf spheroidal galaxies. These are much smaller than spirals and feature luminosities around $\sim 10^5$–$10^6 L_\odot$. Observations indicate that these galaxies are much more dark matter-dominated than spirals.

The cooling rate in dwarf spheroidal galaxies is suppressed if the halo mirror plasma temperature is below around 3 eV. For such temperatures Fig. 2 indicates that most of the mirror helium would be in neutral atoms. Only the smaller mirror hydrogen subcomponent is ionized and could thereby participate in bremsstrahlung cooling.

The halo temperature for dwarf spheroidal galaxies can be computed in the same way in which we computed the temperature for spirals, discussed in Sec. III. Consider two examples with (a) a dark matter core radius $r_0 = 0.5$ kpc and central density $\rho_0 = 10^{-23}$ g/cm^3 and (b) $r_0 = 0.5$ kpc and central density $\rho_0 = 5 \times 10^{-24}$ g/cm^3. Both examples are consistent with the observations [58]. The results of numerically solving Eq. (9) are shown in Fig. 10. When computing the temperature profile for dwarf spheroidal galaxies, we have neglected the baryon component completely as far as its contribution to the local acceleration, g. This is reasonable because the baryonic mass is estimated to be only a few percent of the total mass

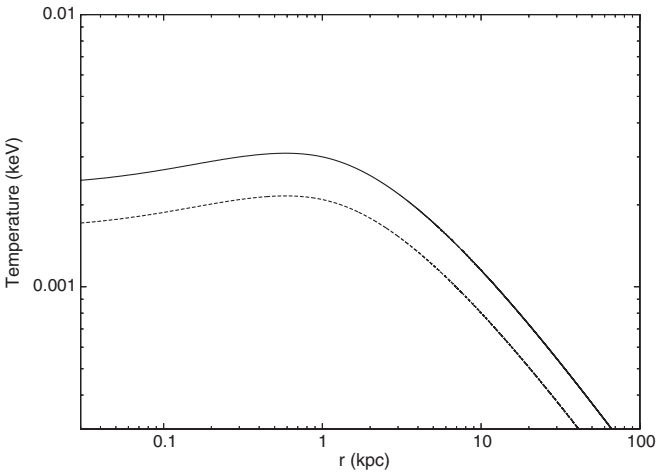

FIG. 10. The mirror plasma temperature profile for a dwarf spheroidal galaxy. Shown is an example with dark matter core radius $r_0 = 0.5$ kpc and central density $\rho_0 = 10^{-23}$ g/cm^3 (solid line). Also shown is another example with the same dark matter core radius $r_0 = 0.5$ kpc but a slightly higher central density, $\rho_0 = 5 \times 10^{-24}$ g/cm^3 (dashed line).

for these galaxies [58]. Note that for both examples, Fig. 2 indicates that only a small proportion of mirror helium will be fully ionized. [Numerically we find that example (a) has a mean mass parameter given by $\bar{m} \simeq 1.6$ GeV, while example (b) has $\bar{m} \simeq 2.3$ GeV.]

Importantly, dwarf spheroidal galaxies appear to have relatively little ordinary gas component and do not exhibit current star formation [59]. Thus, for dwarf spheroidal galaxies it does not seem possible to stabilize a spherical mirror plasma component with energy from an ordinary supernova. Some other energy source would be needed, or possibly the mirror dark matter has collapsed into a disk/bulge component for this galaxy class.

VII. ELLIPTICAL GALAXIES AND CLUSTERS

Elliptical galaxies are another interesting class of objects to think about. As with dwarf spheroidal galaxies, elliptical galaxies appear to be largely devoid of gas and do not exhibit significant star formation at the present epoch. Thus the current rate of ordinary supernovae is very low. In the absence of supernova heating, the mirror particle plasma is expected to undergo gravitational collapse onto a disk/bulge. For large elliptical galaxies, the time scale for this to occur can be long, and even today many such galaxies might not be fully collapsed. In any case, in the absence of a significant heat source it is reasonable to expect the dark matter within elliptical galaxies to be flattened out, to some extent, due to dissipative processes. This picture is consistent, at least qualitatively, with the observed ellipticity of elliptical galaxies; see e.g. Ref. [60]. That is, for mirror dark matter, and closely related hidden-sector models, the nonspherical distribution of the dark matter in elliptical galaxies can potentially be explained due to dissipation effects (in the absence of which, the observed ellipticity could have been used to place stringent limits on dark matter self-interactions, as in e.g. Ref. [18]).

Within larger structures, such as clusters of galaxies, mirror dark matter self-interactions might lead to important effects. In particular, observations of the Bullet Cluster have been used to argue for stringent constraints on dark matter self-interactions [61]. We recall that the Bullet Cluster is an example of a system in which a collision between two clusters has apparently taken place. Each cluster has three components: the galaxies, hot intergalactic gas and dark matter. When the main cluster and subcluster collide, the hot (ordinary-matter) gas associated with the two colliding clusters appears to be slowed, but not stopped, by interactions. Both the galaxies and dark matter components appear to pass through each other. These observations pose a potential puzzle for mirror dark matter. Why does the dark matter within each cluster not slow down due to interactions? Part of the explanation could be that the fraction of dark matter existing as hot gas unbound to individual galaxies (i.e. intergalactic gas) might be less than the corresponding fraction for ordinary matter [62]. Another part of the explanation could be that mirror dark matter has self-interactions which are weaker than those of ordinary matter due to environmental conditions, in particular, if the mirror particle plasma has a higher temperature than the ordinary particle plasma. Recall that the mirror electron scattering cross section behaves like $d\sigma/d\Omega \propto 1/v^4 \sim 1/T^2$. The temperature, T, of the mirror particle plasma is uncertain, but the hydrostatic equilibrium condition, Eq. (9), suggests that $T \propto \bar{m}$. The higher helium mass fraction in the mirror sector means that $\bar{m} \approx 1.1$ GeV for mirror dark matter, cf. $\bar{m} \approx 0.55$ GeV for ordinary matter, and thus the temperature of the mirror plasma in clusters might be higher than that of the ordinary plasma by a factor of around two or so. If this is indeed part of the explanation of the Bullet Cluster observations, then studies of colliding clusters which feature lower temperatures could find an offset between the galaxy component and the total mass distribution. Interestingly, there are some tentative hints in this direction [63].

VIII. CONCLUDING REMARKS

We have examined galactic structure within the context of dissipative dark matter candidates, focusing on the mirror dark matter model. At first sight, dissipative dark matter might seem unlikely, given the inferred approximate sphericity of dark matter halos in spiral galaxies. However, the idea [33] that there exists a heat source to counteract the halo cooling due to dissipative interactions and that this heat source could be an ordinary supernova seems to be possible. At any rate, it is a specific idea, and mirror dark matter offers a specific model in which to study it.

In this article we have provided a detailed numerical analysis of this whole picture. Although a number of assumptions are made, and a few corners may have been cut, our results are very encouraging. Our analysis indicates that the inferred dark matter scaling properties of spiral galaxies, discovered by Salucci and others, are explicable within this dark matter framework. Moreover our results are remarkably insensitive to many of the unknown parameters of the theory (such as details of the supernova energy spectrum, mirror metal mass fraction, etc.). Thus, we have reason to be confident that this dissipative dark matter picture, and to some extent the specific mirror dark matter implementation of it, may well be on the right track in explaining galactic structure. That is, we agree with the title of Ref. [3], "Dark matter in galaxies: leads to its nature."

ACKNOWLEDGMENTS

This work was supported by the Australian Research Council.

[1] For a review, see e.g. S. Dodelson, *Modern Cosmology* (Academic Press, Amsterdam, 2003).

[2] G. F. Smoot *et al.*, Astrophys. J. **396**, L1 (1992); G. Hinshaw *et al.*, arXiv:1212.5226; R. Keisler *et al.*, Astrophys. J. **743**, 28 (2011); J. L. Sievers *et al.*, arXiv:1301.0824; P. A. R. Ade *et al.* (Planck Collaboration), arXiv:1303.5076.

[3] For a review, see e.g. P. Salucci and M. De Laurentis, arXiv:1302.2268.

[4] J. F. Navarro, C. S. Frenk, and S. D. M. White, Astrophys. J. **462**, 563 (1996); B. Moore, T. R. Quinn, F. Governato, J. Stadel, and G. Lake, Mon. Not. R. Astron. Soc. **310**, 1147 (1999).

[5] G. Aad *et al.* (ATLAS Collaboration), Phys. Lett. B **709**, 137 (2012); Phys. Rev. D **87**, 012008 (2013); S. Chatrchyan *et al.* (CMS Collaboration), Phys. Rev. Lett. **107**, 221804 (2011); **109**, 171803 (2012).

[6] S. I. Blinnikov and M. Yu. Khlopov, Sov. J. Nucl. Phys. **36**, 472 (1981); Sov. Astron. **27**, 371 (1983).

[7] E. W. Kolb, D. Seckel, and M. S. Turner, Nature (London) **314**, 415 (1985); H. M. Hodges, Phys. Rev. D **47**, 456 (1993).

[8] A. Y. Ignatiev and R. R. Volkas, arXiv:hep-ph/0306120; R. Foot, Int. J. Mod. Phys. D **13**, 2161 (2004); Int. J. Mod. Phys. A **19**, 3807 (2004); Z. Berezhiani, Int. J. Mod. Phys. A **19**, 3775 (2004); Z. K. Silagadze, Acta Phys. Pol. B **32**, 99 (2001); P. Ciarcelluti, Int. J. Mod. Phys. D **19**, 2151 (2010).

[9] Z. Berezhiani, D. Comelli, and F. L. Villante, Phys. Lett. B **503**, 362 (2001); A. Yu. Ignatiev and R. R. Volkas, Phys. Rev. D **68**, 023518 (2003); Z. Berezhiani, P. Ciarcelluti, D. Comelli, and F. L. Villante, Int. J. Mod. Phys. D **14**, 107 (2005); P. Ciarcelluti, Int. J. Mod. Phys. D **14**, 187 (2005); **14**, 223 (2005).

[10] R. Foot and R. R. Volkas, Phys. Rev. D **68**, 021304 (2003); **69**, 123510 (2004).

[11] H. Goldberg and L. J. Hall, Phys. Lett. B **174**, 151 (1986); L. Ackerman, M. R. Buckley, S. M. Carroll, and M. Kamionkowski, Phys. Rev. D **79**, 023519 (2009); F.-Y. Cyr-Racine and K. Sigurdson, Phys. Rev. D **87**, 103515 (2013); J. Fan, A. Katz, L. Randall, and M. Reece, arXiv:1303.1521.

[12] J. M. Cline, Z. Liu, and W. Xue, Phys. Rev. D **85**, 101302 (2012).

[13] N. F. Bell, K. Petraki, I. M. Shoemaker, and R. R. Volkas, Phys. Rev. D **84**, 123505 (2011); K. Petraki, M. Trodden, and R. R. Volkas, J. Cosmol. Astropart. Phys. 02 (2012) 044.

[14] R. N. Mohapatra and V. L. Teplitz, Phys. Rev. D **62**, 063506 (2000); R. N. Mohapatra, S. Nussinov, and V. L. Teplitz, Phys. Rev. D **66**, 063002 (2002).

[15] J.-W. Cui, H.-J. He, L.-C. Lu, and F.-R. Yin, Phys. Rev. D **85**, 096003 (2012); R. Foot, Phys. Lett. B **703**, 7 (2011); arXiv:1209.5602 [Phys. Rev. D (to be published)]; T. Higaki, K. S. Jeong, and F. Takahashi, arXiv:1302.2516.

[16] P.-H. Gu, arXiv:1303.6545.

[17] N. Arkani-Hamed, D. P. Finkbeiner, T. R. Slatyer, and N. Weiner, Phys. Rev. D **79**, 015014 (2009).

[18] J. L. Feng, H. Tu, and H.-B. Yu, J. Cosmol. Astropart. Phys. 10 (2008) 043; J. L. Feng, M. Kaplinghat, H. Tu, and H.-B. Yu, J. Cosmol. Astropart. Phys. 07 (2009) 004.

[19] S. Andreas, M. D. Goodsell, and A. Ringwald, Phys. Rev. D **87**, 025007 (2013); P. Arias, D. Cadamuro, M. Goodsell, J. Jaeckel, J. Redondo, and A. Ringwald, J. Cosmol. Astropart. Phys. 06 (2012) 013.

[20] X. Chu, T. Hambye, and M. H. G. Tytgat, J. Cosmol. Astropart. Phys. 05 (2012) 034.

[21] R. Foot and X-G. He, Phys. Lett. B **267**, 509 (1991).

[22] B. Holdom, Phys. Lett. **166B**, 196 (1986).

[23] R. Foot, H. Lew, and R. R. Volkas, Phys. Lett. B **272**, 67 (1991); Mod. Phys. Lett. A **07**, 2567 (1992); R. Foot and R. R. Volkas, Phys. Rev. D **52**, 6595 (1995); Related concepts were discussed prior to the advent of the standard model in T. D. Lee and C. N. Yang, Phys. Rev. **104**, 256 (1956); I. Kobzarev, L. Okun, and I. Pomeranchuk, Sov. J. Nucl. Phys. **3**, 837 (1966); M. Pavsic, Int. J. Theor. Phys. **9**, 229 (1974).

[24] P. Ciarcelluti and R. Foot, Phys. Lett. B **679**, 278 (2009); R. Foot, Phys. Lett. B **711**, 238 (2012); **718**, 745 (2013).

[25] S. L. Glashow, Phys. Lett. **167B**, 35 (1986); R. Foot and S. N. Gninenko, Phys. Lett. B **480**, 171 (2000); A. Badertscher, P. Crivelli, W. Fetscher, U. Gendotti, S. N. Gninenko, V. Postoev, A. Rubbia, V. Samoylenko, and D. Sillou, Phys. Rev. D **75**, 032004 (2007).

[26] R. Foot, Phys. Rev. D **69**, 036001 (2004); Mod. Phys. Lett. A **19**, 1841 (2004); Phys. Rev. D **78**, 043529 (2008); Phys. Lett. B **692**, 65 (2010); Phys. Rev. D **82**, 095001 (2010); **86**, 023524 (2012); arXiv:1305.4316.

[27] R. Bernabei *et al.* (DAMA Collaboration), Riv. Nuovo Cimento **26**, 1 (2003); Int. J. Mod. Phys. E **13**, 2127 (2004); Phys. Lett. B **480**, 23 (2000); Eur. Phys. J. C **67**, 39 (2010); **56**, 333 (2008).

[28] C. E. Aalseth *et al.* (CoGeNT Collaboration), Phys. Rev. Lett. **106**, 131301 (2011); **107**, 141301 (2011).

[29] G. Angloher *et al.*, Eur. Phys. J. C **72**, 1971 (2012).

[30] R. Agnese *et al.* (CDMS Collaboration), arXiv:1304.4279.

[31] R. Foot and S. Mitra, Astropart. Phys. **19**, 739 (2003); Phys. Lett. B **558**, 9 (2003); Phys. Lett. A **315**, 178 (2003); R. Foot, Acta Phys. Pol. B **32**, 3133 (2001); R. Foot and T. L. Yoon, Acta Phys. Pol. B **33**, 1979 (2002); Z. K. Silagadze, Acta Phys. Pol. B **36**, 935 (2005); S. Mitra, Phys. Rev. D **74**, 043532 (2006).

[32] Z. K. Silagadze, Yad. Fiz. **60N2**, 336 (1997) [Phys. At. Nucl. **60**, 272 (1997)]; R. Foot, Phys. Lett. B **452**, 83 (1999).

[33] R. Foot and R. R. Volkas, Phys. Rev. D **70**, 123508 (2004).

[34] R. Foot and Z. K. Silagadze, Int. J. Mod. Phys. D **14**, 143 (2005).

[35] F. Sandin and P. Ciarcelluti, Astropart. Phys. **32**, 278 (2009).

[36] R. Foot and Z. K. Silagadze, arXiv:1306.1305.

[37] G. G. Raffelt, *Stars As Laboratories For Fundamental Physics: The Astrophysics Of Neutrinos, Axions, And Other Weakly Interacting Particles* (Chicago University Press, Chicago, 1996); S. Davidson, S. Hannestad, and G. Raffelt, J. High Energy Phys. 05 (2000) 003; R. N. Mohapatra and I. Z. Rothstein, Phys. Lett. B **247**, 593 (1990).

[38] R. Foot, arXiv:1303.1727.

[39] B. H. Bransden and C. J. Joachain, *Physics of Atoms and Molecules* (Prentice Hall, Upper Saddle River, USA, 2003).

[40] G. B. Rybicki and A. P. Lightman, *Radiative processes in astrophysics* (Wiley, Hoboken, USA, 2008).
[41] J. Kormendy and K. C. Freeman, arXiv:astro-ph/0407321.
[42] M. Spano, M. Marcelin, P. Amram, C. Carignan, B. Epinat, and O. Hernandez, Mon. Not. R. Astron. Soc. **383**, 297 (2008).
[43] F. Donato, G. Gentile, P. Salucci, C. Frigerio Martins, M. I. Wilkinson, G. Gilmore, E. K. Grebel, A. Koch, and R. Wyse, Mon. Not. R. Astron. Soc. **397**, 1169 (2009).
[44] C. Alcock *et al.* (MACHO Collaboration), Astrophys. J. **542**, 281 (2000); P. Tisserand *et al.* (EROS-2 Collaboration), Astron. Astrophys. **469**, 387 (2007).
[45] P. Ciarcelluti and R. Foot, Phys. Lett. B **690**, 462 (2010).
[46] Z. Berezhiani, S. Cassisi, P. Ciarcelluti, and A. Pietrinferni, Astropart. Phys. **24**, 495 (2006).
[47] P. Salucci, A. Lapi, C. Tonini, G. Gentile, I. Yegorova, and U. Klein, Mon. Not. R. Astron. Soc. **378**, 41 (2007).
[48] M. Persic, P. Salucci, and F. Stel, Mon. Not. R. Astron. Soc. **281**, 27 (1996).
[49] A. Burkert, IAU Symposium/Symp-Int.Astron.Union **171**, 175 (1996); Astrophys. J. **447**, L25 (1995); P. Salucci and A. Burkert, Astrophys. J. **537**, L9 (2000).
[50] R. Foot (to be published).
[51] W. Lotz, Z. Phys. **216**, 241 (1968).
[52] Y. S. Kim and R. H. Pratt, Phys. Rev. A **27**, 2913 (1983) and references therein.
[53] C. Corliss and J. Sugar, J. Phys. Chem. Ref. Data **11**, 135 (1982).
[54] F. Shankar, A. Lapi, P. Salucci, G. De Zotti, and L. Danese, Astrophys. J. **643**, 14 (2006).
[55] F. Donato and P. Salucci, Mon. Not. R. Astron. Soc. **353**, L17 (2004).
[56] W. Li, R. Chornock, J. Leaman, A. V. Filippenko, D. Poznanski, X. Wang, M. Ganeshalingam, and F. Mannucci, Mon. Not. R. Astron. Soc. **412**, 1473 (2011).
[57] J. S. Gallagher, D. A. Hunter, and A. V. Tutukov, Astrophys. J. **284**, 544 (1984).
[58] P. Salucci *et al.*, arXiv:1111.1165.
[59] See e.g. E. K. Grebel, J. S. Gallagher, and D. Harbeck, Astron. J. **125**, 1926 (2003).
[60] D. A. Buote, T. E. Jeltema, C. R. Canizares, and G. P. Garmire, Astrophys. J. **577**, 183 (2002).
[61] M. Markevitch, A. H. Gonzalez, D. Clowe, A. Vikhlinin, W. Forman, C. Jones, S. Murray, and W. Tucker, Astrophys. J. **606**, 819 (2004); D. Clowe, M. Bradač, A. H. Gonzalez, M. Markevitch, S. W. Randall, C. Jones, and D. Zaritsky, Astrophys. J. **648**, L109 (2006).
[62] Z. K. Silagadze, ICFAI Univ. J. Phys. **2**, 143 (2009).
[63] A. Mahdavi, H. Hoekstra, A. Babul, D. Balam, and P. Capak, Astrophys. J. **668**, 806 (2007); M. J. Jee, A. Mahdavi, H. Hoekstra, A. Babul, J. J. Dalcanton, P. Carroll, and P. Capak, Astrophys. J. **747**, 96 (2012).